

Chemical Composition of Galactic Cosmic Rays with Space Experiments

Mirko Boezio¹, Emiliano Mocchiutti

INFN, Sezione di Trieste, I-34149 Trieste, Italy

Abstract

The origin and properties of the cosmic radiation are one of the most intriguing question in modern astrophysics. The precise measurement of the chemical composition and energy spectra of the cosmic rays provides fundamental insight into these subjects. In this paper we will review the existing experimental data. Specifically, we will analyse results collected by space-born experiments discussing the experimental uncertainties and challenges with a focus on the PAMELA experiment.

Keywords: Cosmic rays, Acceleration of particles, Abundances, Space vehicles

1. Introduction

Since the discovery of cosmic rays, the fundamental question concerned their origin, acceleration and propagation mechanisms. From an energetic point of view it was realized in the fifties (e.g. [1]) that Super Nova explosions, already considered as cosmic-ray sources by Baade and Zwicky [2] in the thirties, released sufficient energy to power the cosmic rays in the Galaxy. A viable acceleration mechanism, based on diffusive shock acceleration (“first order Fermi mechanism”) produced by supernova (SN) shock waves propagating in the interstellar medium (see [3] for a review), was proposed in the seventies and recent measurements of synchrotron X-rays and TeV gamma-rays point unambiguously to supernovae remnants (SNR) [4, 5] as the acceleration site of at least cosmic-ray electrons. However, the vast majority of the cosmic rays are protons and heavier nuclei with electrons representing only few percent of the total flux. For example, TeV emission from the young supernova remnant RX J1713.7-3946, detected by the H.E.S.S. collaboration [6], has been interpreted as originating from hadronic interactions of cosmic rays with energies above 10^{14} eV in the shell of the SNR (even though leptonic processes cannot be ruled out [7, 8]). X-ray measurements of the same SNR provide evidence that protons and nuclei can be accelerated to energies $\geq 10^{15}$ eV [9]. Recent AGILE observations of diffuse gamma ray emission in the 100 MeV - 1 GeV range from the outer shock region of SNR IC 443 have been explained in terms of hadronic acceleration [10]. Likewise, Fermi observations of the shell of SNR W44 have been attributed to the decay of π^0 s produced during interactions of accelerated hadrons with the interstellar medium [11].

At the end of the acceleration phase, particles are injected into the interstellar medium where they propagate, diffusing in the turbulent galactic magnetic fields. Nowadays, this propagation is well described by solving numerically (e.g. the GALPROP simulation code [12]) or analytically (e.g. [13, 14]) the transport equations for the particle diffusion in the galaxy. The galactic magnetic field masks the arrival direction of charged particles, making the flux isotropic. Hints of galactic anisotropy have been reported in the multi-TeV region [15, 16, 17, 18].

One of the features predicted by such acceleration and propagation models is that the cosmic-ray spectra are well described by single power laws, with similar spectral indices ($\gamma \simeq -2.7$) for protons and heavier nuclei, up to energies of $\approx 10^{15}$ eV (the so called ‘knee’ region). Till recently, indeed,

observations looked consistent with such picture. More recent acceleration models account for the dynamical interaction between the shock front and accelerated particles. The resulting energy injection spectra are not anymore a single power law but are in general concave presenting a hardening at higher energies (e.g. [19]). Combined with propagation effects, additional structures may appear in the energy spectra of cosmic rays probably in the TeV region with possible spectral differences between the various species (e.g. [20]).

About 50 years ago a clear change in the energy spectrum of cosmic rays was observed around 10^{15} eV [21]. Since then, more data have been acquired confirming the first evidence, but no theoretical explanation have yet been accepted as fully satisfactory by the cosmic-ray community. While yet unclear, the origin of the knee is probably related to the acceleration mechanism. In fact in diffusive shock acceleration model cosmic rays are accelerated in blast waves of SNR and a rigidity ($R = pc/(Ze)$, p being the momentum of a particle of charge Ze)-dependent limit, above which the diffusive shock acceleration becomes inefficient, is predicted. The maximum energy attainable by a nucleus of charge Z may range from $Z \times 10^{14}$ eV to $Z \times 10^{15}$ eV depending on the model and types of supernovae considered [22]. Then, the knee would result from the convolution of the various cutoffs while the spectral composition would become heavier. An alternative explanation of the knee is adopted by models that relate it to leakage of cosmic rays from the Galaxy. In this case the knee is expected to occur at lower energies for light nuclei as compared to heavy ones, due to the rigidity-dependence of the Larmor radius of cosmic rays propagating in the galactic magnetic field [23]. The majority of the data in the knee region have been collected by ground detector arrays that, measuring the secondary particles produced by cosmic rays interacting with the Earth's atmosphere, indirectly determine the energy and composition of the cosmic radiation. At lower energies, up to about 10^{14} eV the cosmic-ray spectra have been directly measured mostly by balloon-borne experiments. Both the statistical and systematic uncertainties of these measurements significantly hinder the interpretation of the data.

The cosmic-ray spectra observed at Earth result from the combined effects of acceleration and propagation. A powerful test of propagation models is the measurement of secondary nuclei (e.g. Boron) that are not end-points of stellar evolution but are produced by the interaction of primary cosmic rays (e.g. Carbon and Oxygen) with the interstellar matter. The comparison between their energy spectra and their parent energy spectra (e.g. the B to C ratio, see Fig. 12 on the left, or the ratio of sub-iron elements to

iron) provides fundamental information about the secondary production and propagation of cosmic rays and their dependence from the cosmic-ray energy (or rigidity).

While convincing, the evidences of SNR as acceleration sites of all galactic cosmic rays are not conclusive and this is especially true for the acceleration mechanisms proposed to explain the cosmic-ray spectrum. Moreover, the paucity of high energy (TeV) data concerning secondary nuclei seriously limits our understanding of the interplay between propagation and acceleration. Furthermore, the recent observations by PAMELA [24], CREAM [25] and ARGO-YBJ [18] point to spectral shapes depending on the nuclei species and deviating from the single power law dependence.

Precise determination of the cosmic-ray fluxes and compositions is of crucial importance for the understanding of astrophysical phenomena taking place in the Galaxy. Moreover, data from space mission are sorely needed since the accurate determination of the chemical composition for balloon-borne experiments is intrinsically limited to the region below a few hundred GeV per nucleon because of uncertainties in the atmospheric corrections (i.e. secondaries produced by cosmic rays interacting with the residual atmospheric overburden).

Here we will review the existing data on the chemical composition of cosmic rays from space-borne experiments, with a special focus on the data produced by the PAMELA experiment [26]. We will analyse the experimental uncertainties and challenges and provide a brief outlook for the future of this experimental field.

2. Proton and Helium data

Measurements of primary cosmic-ray proton and helium nuclei spectra have been performed over the years using different techniques: magnet spectrometers, e.g. [27], and RICH detectors [28] have been used for energies up to 1 TeV/n, while calorimetry measurements extended to higher energies, e.g. [29]. The majority of these results, especially concerning the high-energy (> 1 GeV) part of the spectra, were obtained by balloon-borne experiments. Primary cosmic-ray data from space-borne experiments refer mostly to energies lower than 1 GeV. For example, the series of IMP (Interplanetary Monitoring Platform) spacecrafts and especially the University of Chicago's Cosmic Ray Nuclear Composition experiment aboard the IMP-8 satellite [30] measured the energy spectra and chemical composition of cosmic rays up to ~ 100 MeV. While providing relevant information concerning the inner heliospheric condition and effects of solar activity on the cosmic radiation, the data are of less immediate use for studies of galactic cosmic rays. In fact, the solar wind significantly affects the low energy part of cosmic rays, as it can be easily verified monitoring the time variation of the cosmic-ray fluxes and their dependence with the sun activity. As an example Fig. 1 shows the yearly low energy proton flux measured by PAMELA from July 2006 till December 2009, i.e. during the last extended solar minimum. The flux variation with time can be clearly seen as well as the decreasing significance of the variation as the energy increases, becoming negligible above 5 GeV.

The interplay between solar wind and cosmic radiation in the heliosphere is a relevant and fundamental problem in space plasma physics, heliospheric physics and in cosmic ray physics. This is a very active field complementing state-of-the-art numerical models (e.g. [32]) with a significant amount of new data. The heliosphere is the only astrophysical system which is accessible to in-situ spacecraft measurements and its modeling can also lead to fundamental insights applicable to larger astrophysical systems. When the transport and modulation of cosmic rays in the heliosphere will be fully understood it will be possible to infer the local interstellar spectra of cosmic rays down to very low energies (tens of MeV) thus enabling significant conclusions on cosmic ray acceleration and propagation mechanisms (e.g. [33]). However, the existing theoretical and experimental data are not yet sufficiently precise to disentangle the galactic and heliospheric effects on the low energy cosmic radiation. On the other hand, the solar effects on the cosmic-ray energy spectra above several GeV are sufficiently low (Fig. 1) that these data can

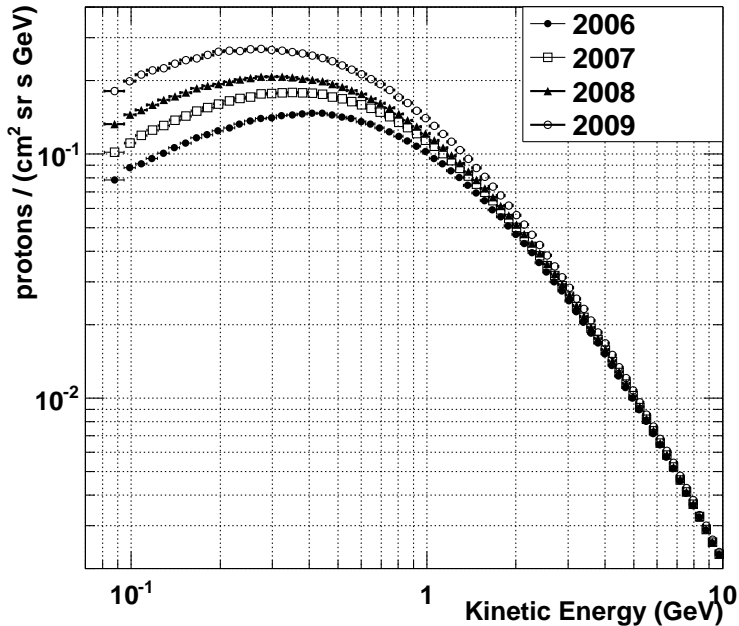


Figure 1: The yearly proton energy spectrum measured by PAMELA from the beginning of the space mission in mid of 2006 till end of 2009 [31].

be considered unbiased samples of the local interstellar spectra.

Figure 2 shows the proton and helium energy spectra¹ above 1 GeV/n measured by recent balloon- [25, 27, 34, 35, 36, 37] and space-borne [24, 38] experiments. Several conclusions can be drawn from these data:

- the high energy (above 1 TeV/n) measurements can be reconciled with the lower energy data only assuming a hardening of the spectra in the hundred GeV region as explicitly indicated by PAMELA and ATIC-2 results;
- the most recent data from PAMELA [24] and CREAM [25] show spectral differences between the proton and helium nuclei.

¹As usually done, the fluxes are multiplied by $E^{2.7}$, where E is the energy in GeV. Reducing the decades of variation of the flux, this allows for a clearer picture of the spectral shapes. However, this implies that the absolute energy uncertainties are added to the flux uncertainties.

- all sets of results are in relatively good agreement, but differences well beyond the quoted statistical-only errors can be noticed at high energies²;

The first two results are interesting and compel a revision of the paradigm of cosmic ray acceleration in supernova remnants followed by diffusive propagation in the galaxy. The discussion about the possible interpretations is beyond the scope of this work. However, as a short summary, these results may indicate that the SNR paradigm has to be better understood as, for example, including the stochasticity in the spatial and temporal distribution of SNR [20]. Or different populations of cosmic-ray sources should be considered such as, for example, novae stars and explosions in superbubbles [39], different acceleration sources for protons and helium and heavier nuclei [40].

Here we will discuss the experimental challenges and significances of these measurements in light of the last two points presented above.

2.1. Systematic Uncertainties

Proton and helium nuclei are usually experimentally identified by measuring their ionization losses in charge sensitive detectors such as plastic scintillators or silicon-array detectors. Since they are the two most abundant components in the cosmic radiation, a charge selection is sufficient to provide clean proton and helium nuclei samples with negligible contamination of other particles (positrons for proton measurements in space, muons for proton measurements at balloon altitude, accounting for a percent or less of high-energy protons). The only significant contamination is of protons in the helium sample and viceversa. This can be reduced to a negligible amount by using redundant ionization measurements. Therefore, the reason for the differences in the experimental measurements, as seen in Fig. 2, cannot be due to background issues.

For the balloon measurements, an additional systematic uncertainty is related to the correction for the residual atmospheric overburden, both as production of secondaries and losses due to interaction. However, this correction usually amounts to less than 10% with a consequent per-cent uncertainty on the estimated flux.

²Below 10 GeV, the difference between the various results is mainly due to solar modulation effects, since the experiments were performed at different epochs of solar activity.

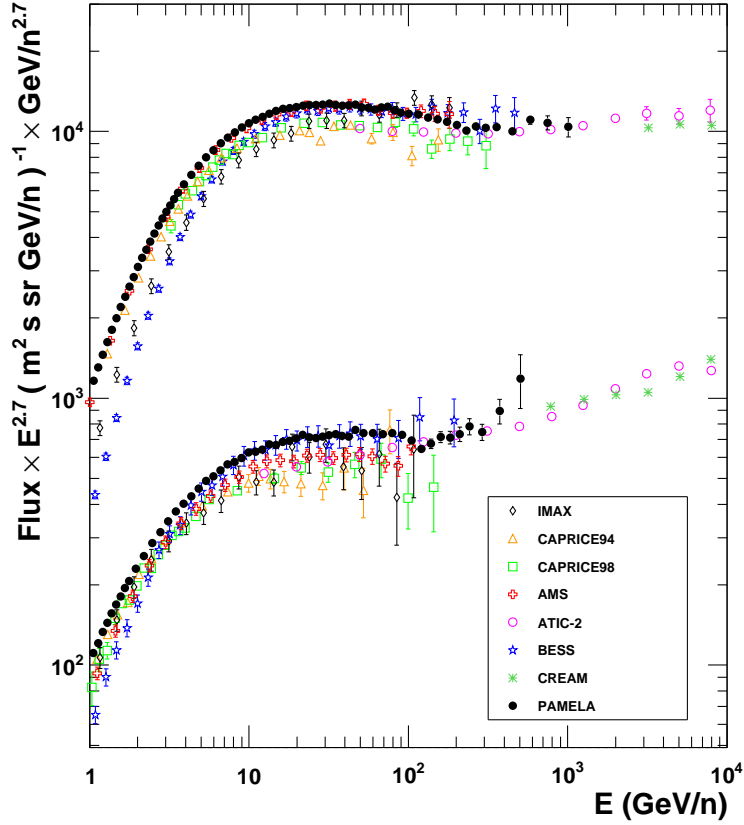


Figure 2: Recent results on the proton and helium energy spectra above 1 GeV/n obtained by balloon-borne: CAPRICE94 [27], IMAX [34], CAPRICE98 [35], BESS [36], ATIC-2 [37], CREAM [25], and space-borne: AMS-01 [38], PAMELA [24] experiments.

Quite likely the main sources of discrepancy arise from efficiency and energy determinations. Selection efficiencies are an experimental challenge since they require a very good knowledge of the detector performances during data taking. Often, to reduce the systematic uncertainties, the selection efficiencies are derived from flight data, but a fully unbiased cross calibration of the efficiencies in flight is quite impossible and simulations have to be used. The simulations are validated by comparisons with test-beam data, which do not account for the flight condition, and, whenever possible, flight data.

However, unproven assumptions have to be made resulting in uncertainties that have to be included in the results. It has to be noted that efficiency uncertainty usually affects the absolute normalization of the fluxes and have a smaller impact on the shape of the spectra.

Another major possible source of discrepancies between the measurements is the energy determination. In the two satellite experiments (AMS-01 and PAMELA) the energy, or more precisely the rigidity, was determined measuring the curvature of charged particles in a magnetic spectrometer. In both cases the particle tracks were reconstructed interpolating position points measured in silicon tracking devices inserted in the magnetic field of permanent magnets. The relevant quantity for this measurement is the Maximum Detectable Rigidity (MDR) defined as the rigidity for which the relative error on the rigidity $\Delta R/R = 100\%$. The momentum resolution and MDR of the magnetic spectrometer depend on the spatial resolution in the bending view and on the topology of the event.

The PAMELA case. For each event the track fitting procedure determined the deflection ($\pm 1/R$) of the particle. The error associated with the measured deflection was used as an estimate of the MDR for each event. This MDR varied from 200 GV to about 1.5 TV according to the distance between the two most distant silicon tracking layers with a detected signal of the reconstructed track. The presented results (Fig. 2) were obtained using events for which the measured rigidity was smaller than the estimated MDR (hence: $R < \text{MDR}$). Consequently, the reconstructed energy spectra had to be unfolded for the varying and increasing, as the rigidity increases, errors on the event deflections. The unfolding procedure used a standard Bayesian approach as described in [41]. This procedure relied on a simulation of the apparatus, which was validated by comparing the distributions of several significant variables (e.g. coordinate residuals, chi-square and the covariance matrix from the track fitting) with those obtained from real data. A systematic uncertainty, estimated folding and unfolding a known spectral shape with the spectrometer response, of 2% was added to the data. Since a clear break in the experimental spectra is found around 200 GV, one may wonder if it results from an incomplete unfolding of the spectra. An important ingredient for a proper definition of the unfolding procedure is the tracking alignment. In fact, a wrong assumption on the absolute position of the tracking sensor respect to the magnetic field results in a wrong measurement of the deflection, essentially appearing as an offset in this measurement.

In experiments like PAMELA and AMS precise alignments of the tracking system (e.g. [42]) were performed at particle test beam facility prior the launch. However, the alignment procedure had to be repeated to account for possible changes in the flight configuration due to the significant shocks and vibrations the apparatus underwent during the operations of launch and placement in orbit. Furthermore, all experiments could be affected by a wrongly mapped magnetic field (especially important for strongly inhomogeneous magnetic fields, e.g. [27]). One possible way to constrain this effect is a redundant energy information. For example, the CAPRICE98 collaboration compared the particle rigidity reconstructed by a magnetic spectrometer with the particle velocity derived by measurements of Cherenkov angles obtained with a gaseous RICH detector [35]. In the PAMELA experiment no such comparison was available for protons and helium nuclei but it was possible for electrons and positrons using the electromagnetic calorimeter. The 16 radiation length PAMELA calorimeter [43] was designed to sample the total energy deposited by electromagnetic showers, hence for these particles it provided a systematically independent energy estimation respect to the rigidity measurement. Furthermore, a deflection offset would act oppositely for electrons and positrons resulting, in case of a positive shift in deflection, in an overestimation (underestimation) of the rigidity for electrons (positrons). On the other hand, the energy measured by the electromagnetic calorimeter is insensitive respect to the charge sign of electrons. Therefore, the comparison between energy measured by the calorimeter and rigidity obtained by the tracking system for both electrons and positrons provided a constrain for global distortions of the tracking system. These would mimic a track curvature and result in a deflection offset, applicable to all particles species. The previous method applied to PAMELA data limited this offset to 10^{-4} GV⁻¹. The corresponding uncertainty was included in the published results [24].

Figure 3 shows the proton and helium rigidity spectra measured by PAMELA [24]. The shaded areas represent the overall (flux and rigidity) estimated systematic uncertainty. For protons these uncertainties dominate the statistical ones at high energy as expected from the previous discussion. While large, however, they cannot explain the difference with the helium spectrum measured by AMS-01 [38] and other balloon experiments [27, 34, 35] as shown in Fig. 2. However, it has to be noted, that the experimental errors in Fig. 2 are only statistical, hence the residual difference may be due to systematic uncertainties of the other experiments. For example, CAPRICE94 [27] quoted a systematic uncertainty of 10% at high energies.

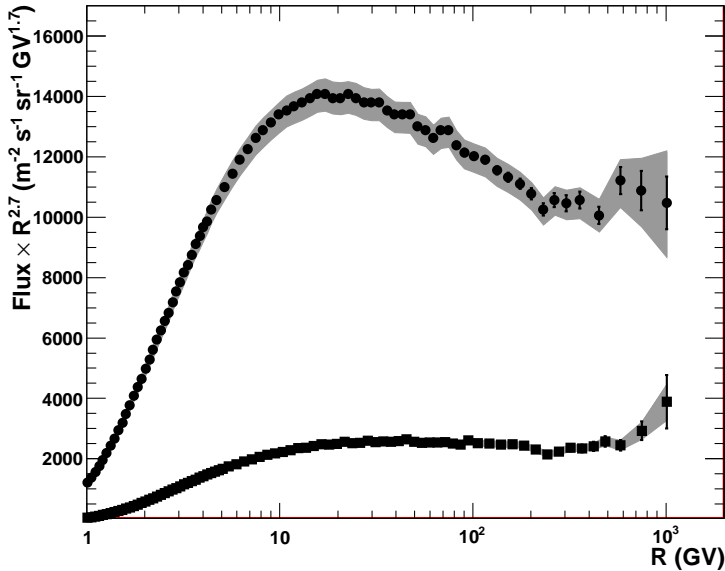


Figure 3: Proton (full circles) and helium (full boxes) fluxes measured by PAMELA [24]. The shaded areas represent the overall (flux and rigidity) estimated systematic uncertainty.

Since they are comparable to the statistical errors, systematic uncertainties have to be included in any interpretation of the experimental data. In the case of PAMELA proton results, the hardening of the spectra around 200 GV has only a 95% confidence level significance when systematic errors are included [24], instead of a 99.7% CL if only statistical errors are considered. Furthermore, there is no clear recipe for including systematic errors with statistical ones. The PAMELA collaboration decided to quadratically sum the systematic uncertainties, in the fair assumption of independence of the errors. Then, it studied the case in which they were added or subtracted to the experimental data, i.e. assuming that they acted uniformly in one or the other direction like maximum errors. More significant is the PAMELA proton to helium flux ratio since, when expressed as a function of rigidity, various systematic uncertainties related to the track measurements cancel out. In this case the hypothesis of a constant value for this ratio is incompatible with the data above 10 GV at a level of about 9 standard deviations.

Another effect, albeit less significant, should be considered when compar-

ing experimental data to theoretical calculations: the experiments cannot separate, except for small energy ranges, the isotopes. Therefore, what is commonly called proton spectrum is in reality a hydrogen one. Furthermore, for measurements with magnetic spectrometer the conversion from rigidity to kinetic energy is performed assuming pure proton and ${}^4\text{He}$ samples, hence neglecting any contribution from less abundant deuterium (${}^2\text{H}/{}^1\text{H} \simeq 1\%$) and ${}^3\text{He}$ (${}^3\text{He}/{}^4\text{He} \simeq 10\%$).

2.2. Proton and helium isotopes

Hydrogen and helium isotopes in cosmic rays are generally believed to be of secondary origin, resulting mainly from the nuclear interactions of primary cosmic-ray ${}^4\text{He}$ with the interstellar medium. Among several secondary components the specific feature of light secondaries such as ${}^2\text{H}$ and ${}^3\text{He}$ is that their interaction mean free path is considerably larger than the escape mean free path for cosmic rays from the Galaxy. This is not the case for the heavier secondaries, where the escape mean free path is of the same order or greater than their interaction length. As a consequence, light secondaries provide information concerning cosmic-ray interstellar propagation that is complementary to that obtained from the study of heavy secondaries and their precise measurement could tell if the helium nuclei have the same propagation history as heavier nuclei (e.g. [44]).

Figure 4 shows the existing data on the ${}^3\text{He}/{}^4\text{He}$ and ${}^2\text{H}/{}^4\text{He}$ ratios. Isotopes separation was achieved by the mean of rigidity versus time-of-flight selections. As it can be seen most of the measurements were obtained below a few GeV nucleon^{-1} of kinetic energy, mostly by balloon-borne experiments [45, 46, 47, 48, 49] and two [50, 51] by space-borne apparatus. In this energy domain data are affected by solar modulation and, in the case of balloon-borne experiments, by a large atmospheric background.

A simple approach for interpreting the data is using the leaky box model [44]. According to this model the propagation of cosmic rays is described by only one energy-dependent parameter, the escape mean free path, which represents the mean amount of matter traversed by cosmic rays before escaping from the confinement volume. Then, the comparison between experimental data and the expected abundances of light secondaries, obtained tuning this parameter on the heavier nuclei component, is a powerful test if their propagation history is actually the same as that of heavier nuclei. Similarly the data can be compared to more sophisticated theoretical calculations such as those based on the GALPROP code [12] (lines in Fig. 4 at different solar

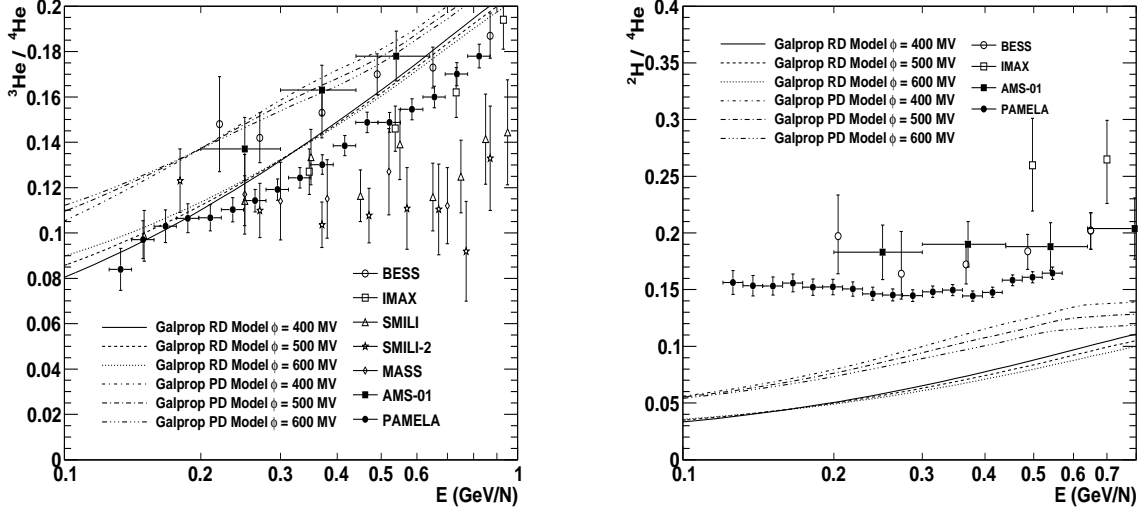


Figure 4: Measurements for the ${}^3\text{He}/{}^4\text{He}$ (left) and ${}^2\text{H}/{}^4\text{He}$ (right) ratios. Most data are from balloon-borne experiments: MASS [45], SMILI [46], SMILI2 [47], IMAX 92 [48], BESS 98 [49] with the exception of the AMS-01 [50] and the preliminary PAMELA [51] results.

modulation parameter ϕ). However, the uncertainties on solar modulation significantly affects the interpretation of the results and data would be needed at energies where these effects are negligible. Till now, only one measurement [52] on the deuterium abundance exist above $10 \text{ GeV nucleon}^{-1}$ but still obtained with a balloon-borne experiment, hence affected by uncertainties on the atmospheric background. Recently, the AMS experiment [53] was placed on board the International Space Station. More details will be provided in Section 6, but the combination of a magnetic spectrometer with an acrylic Ring Imaging Cherenkov should extend the light isotopes measurements up to about 10 GeV/n .

3. Electron data

Electrons (and positrons) constitute about 1% of the total cosmic-ray flux. While small, this component provides important information regarding the origin and propagation of cosmic rays in the Galaxy that is not accessible from the study of the cosmic-ray nuclear components due to their differing energy-loss processes. In fact, because of their low mass, electrons undergo severe energy losses through synchrotron radiation in the Galactic magnetic field and inverse Compton scattering with the ambient photons.

Cosmic-ray electrons and positrons are produced as secondaries by the interactions between cosmic-ray nuclei and the interstellar matter. In this case, they are the end product of the decay of short-lived particles (mostly pions via the decay $\pi^\pm \rightarrow \mu^\pm \rightarrow e^\pm$) produced in interactions. Notice that the positrons are produced in slight excess. Since the observed positron component is of the order of ten percent and less of the electron one above a few GeV (e.g. see [54]), the majority of electrons must be of primary origin. As previously stated, X-ray and TeV gamma-ray measurements point unambiguously to SNRs [4, 5] as acceleration sites of cosmic-ray electrons. However, additional sources of electrons cannot be excluded. Indeed, astrophysical objects such as pulsars, e.g. [55], or more exotic sources such as dark matter particles, e.g. [56], were invoked to explain the positron fraction measured by PAMELA [54] and are expected to contribute to the cosmic radiation with roughly equal numbers of electrons and positrons.

More than in the case of the cosmic-ray nuclear component, structures in the shape of the electron energy spectrum are expected as a contribution of large energy losses and, possibly, of the new sources [33, 57].

In the recent years this field has gained greatly from the addition of new experimental results from ground based [58], balloon-borne [59] and satellite-based experiments. Especially the results from the space-borne Fermi [60] and PAMELA [61] experiments have been particularly significant.

Figure 5 shows the electron energy spectrum measured by PAMELA and Fermi and other recent balloon and space born experiments [59, 62, 63, 64, 65, 66, 67] and a theoretical calculation of the e^- spectrum based on the GALPROP code [12]. The calculation (solid line) was performed using a spatial Kolmogorov diffusion with spectral index $\delta = 0.34$ and diffusive reacceleration characterized by an Alfvén speed $v_A = 36$ km/s, the halo height was 4 kpc (parameters from [68]). The resulting flux was normalized to PAMELA data at ~ 70 GeV. For the secondary e^- production during propagation

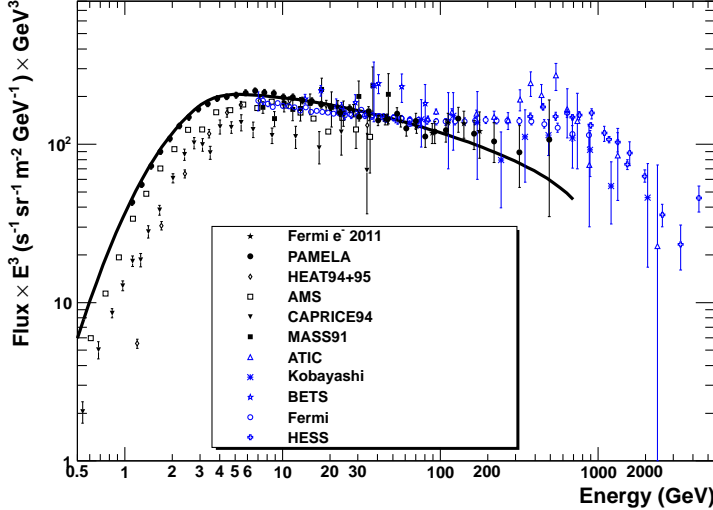


Figure 5: The electron energy spectrum from Fermi [60] and PAMELA [61] with contemporary measurements: Kobayashi [66], CAPRICE94 [62], HEAT [64], BETS [67], AMS [63], MASS91 [65], ATIC [59], HESS [58] and a theoretical calculation based on the GALPROP code [12] (solid line). Note that the data from [58, 59, 60, 66] and the highest data point from HEAT [64] are for the electron and positron sum.

it used primary proton and helium spectra reproducing the corresponding measured PAMELA spectra (see Fig. 2) and it was calculated for solar minimum, using the force field approximation [69] ($\Phi = 600$ MV). It should be mentioned that GALPROP does not fully describe cosmic-ray electron propagation. This calculation is commonly used assuming a continuous distribution of sources in the Galaxy. However, due to the significant energy losses this does not seem plausible for primary high energy electrons, which probably originate from a small number of sources well localized in space.

Both Fermi and PAMELA data show a rather smooth energy dependence of the energy spectra in a relatively good agreement with the GALPROP calculation except at higher energies where the experimental spectra are harder. Such observation was already made by the Fermi collaboration in their first publication [70]. They concluded that data and calculation could be reconciled assuming a harder electron injection spectrum at the source. For example Ahlers et al. [71], following the proposal of Blasi [72], considered the production and acceleration of secondaries electrons and positrons by

hadronic interactions of the accelerated protons in SNR shock waves. With such assumption, they were able to fit the Fermi (and HESS) electron data and, at the same time, reproduce the increase in the positron fraction measured by PAMELA [54]. However, additional sources could also explain the hardening of the electron spectra above 70 GeV and as well explain the increase in the positron fraction. For more detailed discussion see [73].

It can be noticed that the Fermi spectrum [60] is lower as absolute value around 10 GeV than PAMELA data and harder at higher energies. Therefore, the question of consistency between the two sets of measurements has to be addressed before a detailed interpretation of the experimental results. First of all, it is important to notice that the Fermi data [60] refer to the sum of electron and positron fluxes while the PAMELA results refer only to the e^- flux. Therefore, we constructed a PAMELA “all electron” ($e^- + e^+$) spectrum using the PAMELA e^- data [61] and positron fraction [74]. Figure 6, left panel, shows the Fermi and PAMELA all electron data up to

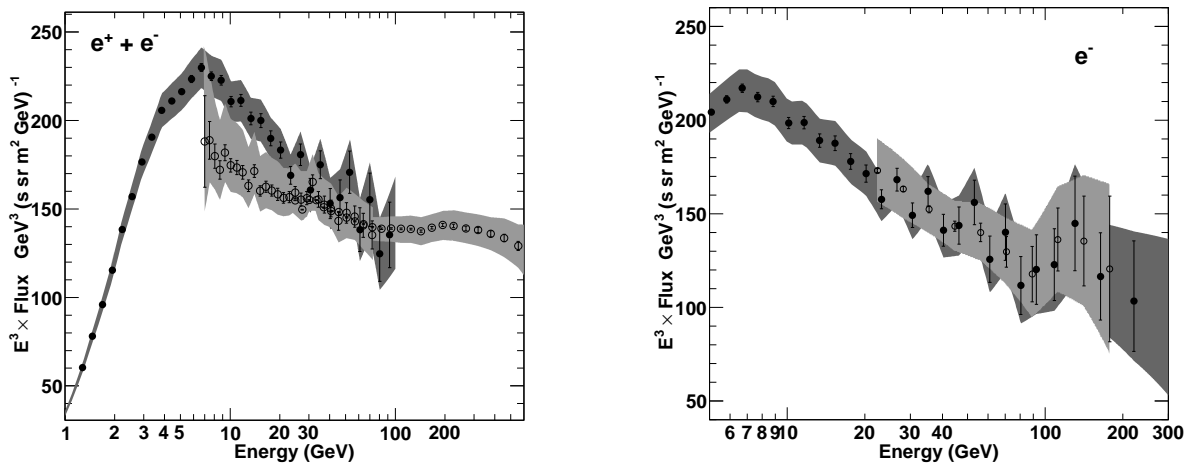


Figure 6: Left panel: the all ($e^- + e^+$) electron energy spectrum from Fermi [60] (open circles) and PAMELA [61, 74] (full circles). The shaded areas represent the overall estimated systematic uncertainties on the fluxes. Right panel: the pure e^- energy spectrum from PAMELA [61] (full circles) and Fermi [75] (open circles), error bars represent the overall estimated systematic uncertainties on the fluxes. Because of the presentation of the fluxes multiplied by E^3 , there are additional systematic uncertainties (not shown here) due to the energy resolution. These amount to 4% at 10 GeV increasing to 13% at 100 GeV for PAMELA and to -10%,+5% for Fermi data.

100 GeV, i.e. the highest energy bin for which the PAMELA collaboration presented the positron fraction. The PAMELA spectrum appears softer than the Fermi one, however the two spectral indexes differ of less than a standard deviation (-3.17 ± 0.07 for PAMELA and -3.112 ± 0.002 for Fermi) when fitting the data with a single power-law from 30 to 100 GeV and accounting only for statistical errors. The difference in shape is not significant even if the two sets of fluxes are increased or decreased in line with the systematic uncertainties: -3.17 ± 0.07 for PAMELA and -3.110 ± 0.002 for Fermi and -3.17 ± 0.07 for PAMELA and -3.132 ± 0.002 for Fermi, respectively. At lower energies, the electron flux measured by PAMELA is higher (about 20% at 10 GeV) than that measured by Fermi. Considering that the data were collected partially over the same period of time the differences cannot be ascribed to solar modulation. However, it should be noted that the systematic uncertainties, shown as shaded areas in Fig. 6, account for most of the differences. Therefore, the two measurements can be considered in agreement. Recently the Fermi collaboration released a measurement of the negative electron spectrum [75] showing an improved agreement with PAMELA results. Making use of the Earth magnetic field to determine the curvature of cosmic rays (derived from the arrival direction of the particle into the apparatus, the map of the Earth magnetic field and the location of the satellite, so called “East–West effect”) it was possible to determine the sign of the charge of charged particles for a subset of Fermi data [75]. By this method, the Fermi Collaboration was able to measure, independently but with lower statistics and in a smaller energy window, the e^- , e^+ fluxes and the positron fraction, see section 4. Results on the e^- spectrum are shown in Fig. 6, right panel, compared to the PAMELA ones. An excellent agreement can be noticed in the whole overlapping energy range, even considering statistical errors only.

As in the case of the hadron energy spectra, differences between the various experimental results might be due to efficiency and energy determinations. However, differently from the previous case, as discussed in section 2 PAMELA had redundant determination of the electron (and positron) energy. This can be seen in Figure 7 that shows the PAMELA electron (e^-) spectra obtained deriving the energy from the calorimeter (full circles) and the tracking information (open circles). The energy spectrum derived by the rigidity measured by the magnetic spectrometer was unfolded to the top of the payload similarly to what was done with proton and helium spectra, accounting, however, also for the electron energy losses due to bremsstrahlung while traversing the pressurized container and parts of the apparatus prior

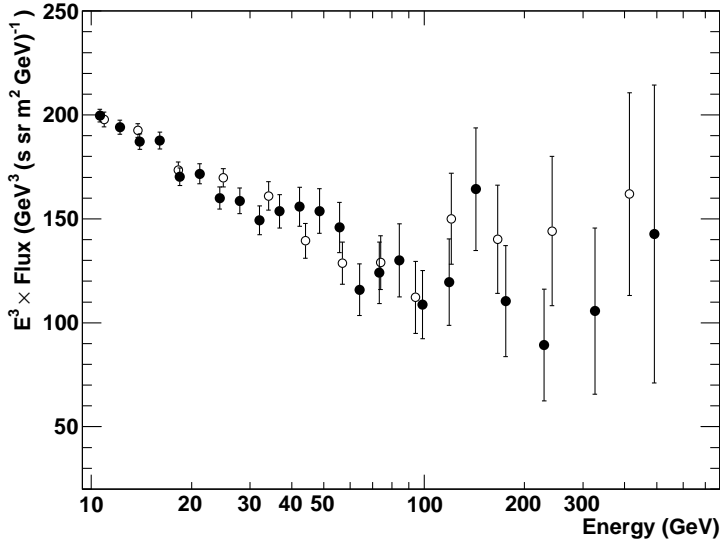


Figure 7: The negatively-charged electron spectrum measured by PAMELA with two independent approaches: energy derived from the calorimeter information (full circles); energy derived from the rigidity (open circles) [61]. The error bars are statistical only.

to the tracking system. In the calorimeter case, tracking information was used solely to select negative particles, thus making a consistency check possible. Such requirement had no effect on the energy reconstruction based on the calorimeter data, while losses due to spillover (i.e. e^+ reconstructed as e^- and, more significant, e^- reconstructed as e^+) were studied with simulation and found negligible below 500 GeV. The two sets of measurements are in good agreement, thus validating both the energy determination and the unfolding procedures [61].

In conclusion, in recent years, especially thanks to new space-borne experiments, there has been a significant improvement in the cosmic-ray electron measurements. The recent data, considering all related uncertainties, are in good agreement both as spectral shape and absolute value of the fluxes. Results, also considering those expected from the AMS experiment, are sufficiently precise to begin for a search of structures expected as contribution of propagation and single sources (e.g. see [33]). This will be the main scientific goal of future satellite-born experiments such as CALET [76] and Gamma-400 [77] that will have the energy resolution and acceptance to precisely

probe the high energy (100s GeV-TeV) region.

4. Antiparticles

Antiparticles (antiprotons and positrons) are a natural component of the cosmic radiation being produced in the interaction between cosmic rays and the interstellar matter. Since the first calculations of secondary antiprotons and positrons (e.g. [78, 79]) antiparticles have been shown to be extremely interesting for understanding the propagation mechanisms of cosmic rays.

Cosmic-ray positrons and antiprotons were first observed in pioneering experiments in the sixties [80] and late seventies [81, 82], respectively, using balloon-borne magnetic spectrometers. While not the only way for detecting antiparticles (e.g. see [83]) magnetic spectrometers provide a clear and simple separation between particles and their antipartners. Figure 8 shows the antiproton energy spectrum (left) and the antiproton-to-proton flux ratio (right) measured by recent cosmic-ray experiments [84, 85, 86, 87, 88, 89, 90] along with theoretical calculations assuming pure secondary production of antiprotons during the propagation of cosmic rays in the galaxy. The experimental data reproduce the falloff below around 2 GeV, characteristic of a secondary spectrum, in the antiproton flux and are in overall agreement with pure secondary calculations. However, it may be noted that the experimental uncertainties, especially of the recent PAMELA experiment [84], are smaller than the spread in the theoretical curves, therefore, pointing to a need for improved calculations.

Figure 9 shows the positron energy spectrum (left) and the positron fraction (right), ratio of positron and electron fluxes (ϕ): $\phi(e^+) / (\phi(e^+) + \phi(e^-))$, measured by recent cosmic-ray space-[63, 74, 75] and balloon-borne [62, 64, 96, 97, 98] experiments. The solid lines show the original calculation by Moskalenko & Strong [12] (calculated using the force field approximation [69] with solar modulation parameter $\Phi = 600$ MV) and the dashed line shows the historic calculation of the positron fraction by Protheroe [79] assuming a pure secondary production of positrons during the propagation of cosmic-rays in the galaxy. Two features are clearly visible in the data. At low energies (below 5 GeV) the contemporary results by PAMELA [74] and by Aesop [98] are systematically lower than other data, and at high energies (above 10 GeV) the PAMELA results show that the positron fraction increases significantly with energy opposite to the expectation for secondary production. Below 5 GeV the contemporary measurements of the positron fraction by PAMELA [74] and Aesop [98] are systematically lower than other data. Above 10 GeV the PAMELA and the subsequent Fermi results show that the positron fraction

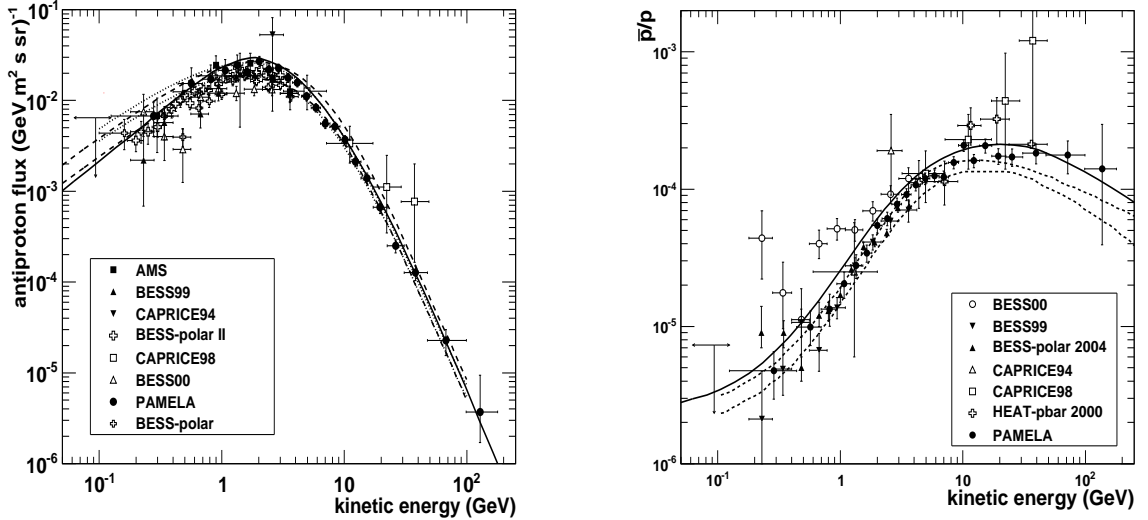


Figure 8: Recent measurements of the antiproton energy spectrum (left): PAMELA [84], CAPRICE94 [85], CAPRICE98 [86], BESS99-00 [88], BESS-polar04 [89], AMS-01 [90], BESS-Polar II [91] and the antiproton-to-proton flux ratio (right): PAMELA [84], HEAT-pbar [87], CAPRICE94 [85], CAPRICE98 [86], BESS99-00 [88], BESS-polar04 [89]. The PAMELA and AMS-01 results are from space-borne experiments. The dotted lines indicate the upper and lower limits calculated by Donato et al. [14, 92] for different diffusion models, including uncertainties on propagation parameters and antiproton production cross-sections, respectively. The solid line shows the calculation by Ptuskin et al. [68] for the case of a Plain Diffusion model. In the multi TeV region upper limits at $\bar{p}/p \sim 0.1$ from EAS experiments (MACRO [93], Tibet AS-gamma [94], ARGO-YBJ [95]) exploiting the moon shadow effect, are not shown in figure. The discussion of these results is beyond the scope of this review.

increases significantly with energy, opposite to the expectation for secondary production. The Fermi results [75] are in relatively good agreement, considering the systematic uncertainties, with PAMELA data. The measured positron fraction is higher but consistent with PAMELA results and show the same increasing trend as the energy increases. Partially moderated by the relatively large uncertainties, this agreement is a positive confirmation of the results especially for what concern all possible sources of systematics due to environmental effects.

The low energy discrepancy between the contemporary results and those from the nineties, i.e. from the previous solar cycle that favored positively-charged particles, are interpreted as a consequence of solar modulation effects

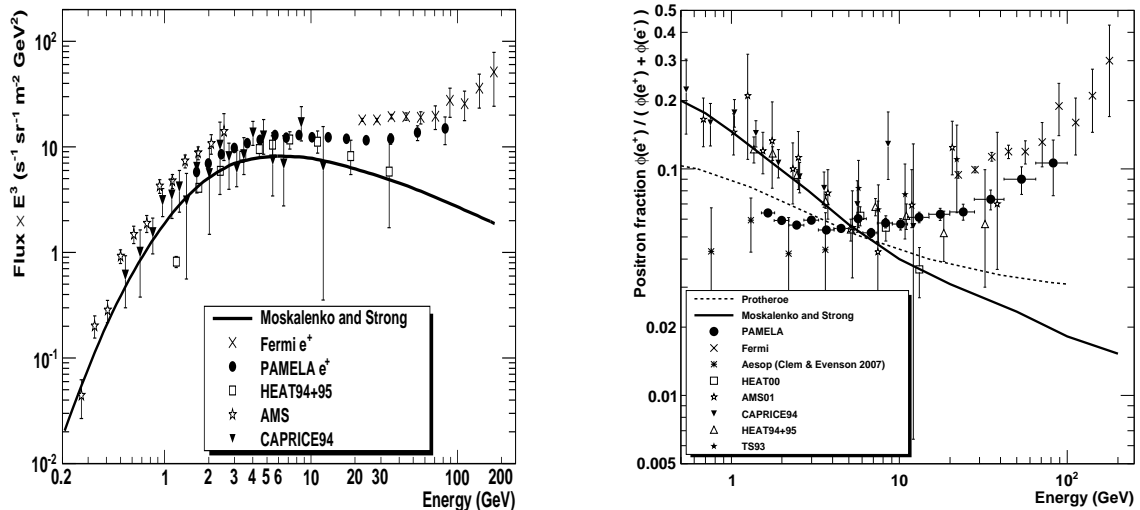


Figure 9: Recent measurements of the positron energy spectrum (left): CAPRICE94 [62], HEAT94+95 [64], AMS-01 [63], PAMELA [61, 74], Fermi [75] and the positron fraction (right): TS93 [96], HEAT94+95 [97], CAPRICE94 [62], AMS-01 [63, 99], Aesop [98], PAMELA [74], Fermi [75]. The PAMELA, AMS-01 and Fermi results are from space-borne experiments. The solid lines show the original GALPROP calculation by Moskalenko & Strong [12] and the dashed line shows the historic calculation of the positron fraction by Protheroe [79] for pure secondary production of positrons during the propagation of cosmic-rays in the galaxy.

(e.g. [100, 101]). The high energy deviation of the experimental data respect to theoretical calculations may indicate the contribution of novel sources for cosmic-ray positrons (and electrons) either of astrophysical (e.g. pulsars [55]) or exotic (e.g. dark matter [56]) origin.

A detailed discussion of the interpretation of these measurements is beyond the scope of this work and the reader is referred to [73]. Instead, here we will discuss the systematic uncertainties related to the experimental data.

As for the case of the electron and proton measurements, efficiency and energy estimations are sources of experimental uncertainties, partially reducible when estimating the ratios or fractions since most of the efficiencies cancel out. However, their role is less significant than that played by the particle identification in a vast background of same charge and sign particles, which are protons for positrons and electrons for antiprotons for space-borne experiments. In fact, the antiproton-to-electron and the positron-to-proton

flux ratio in the cosmic radiation are approximately 10^{-2} and 10^{-3} between 1 and 100 GeV. Additionally, misidentification of electrons as positrons and, especially, protons as antiprotons can occur if the sign-of-charge is incorrectly assigned from the spectrometer data. Furthermore, environmental conditions have to be considered. For example locally produced pions can contaminate the antiproton sample, especially at low energies. Reentrant albedo particles may be mistaken for interstellar cosmic rays if the geomagnetic field of the Earth is not properly treated. In the case of balloon-borne measurements, atmospheric muons are a significant background since they are about an order of magnitude larger than the antiparticle signal. Furthermore, atmospheric secondaries, i.e. produced by interaction of cosmic rays with the residual atmosphere above the payload, comprise an additional irreducibly contamination that can only be estimated by Montecarlo or analytical calculations (e.g. [102]) amounting often to 20% or more of the interstellar antiparticle signal in the GeV region.

Several of these backgrounds have different spectral shapes respect to the signals. Thus, if not completely accounted for, they may mimic changes in energy spectra and, consequently, produce a positron fraction or an antiproton-to-proton flux ratio that increases with energy.

As an example, to understand the level of contamination that might lead to a misinterpretation of the positron data, we analyse one energy interval from PAMELA data. Figure 10 shows the fraction of calorimeter energy deposited inside a cylinder of radius 0.3 Molière radii [103], with axis defined by extrapolating the particle track reconstructed in the spectrometer. Three cases are shown (see [101] for more details):

- (a) positively-charged particles;
- (b) positively-charged particles selected requiring a match between the momentum measured by the tracking system and the total detected energy and the starting point of the shower in the calorimeter;
- (c) negatively-charged particles selected as in (b).

for events with rigidity measured between 28 and 42 GV. In this rigidity range and for an acquisition time of about three and half years, with the procedure described in Adriani et al. [74], 64.2 positron events were estimated. The expectation according to GALPROP prediction was for about 18 events. Considering that there were ~ 250000 positive events in this

interval (panel (a)), a residual proton contamination of $\sim 2 \times 10^{-4}$ could account for the larger estimated value. While this contamination value does not look unreasonable, it is worth pointing out that with simple conditions on the energy deposit in the calorimeter³ only 215 positive, panel (b), and 821 negative, panel (c), events remain. As can be seen in Fig. 10, there is a clear similarity between the distributions in panels (b) and (c). There are corresponding peaks that can be naturally associated to positrons and electrons, respectively, and a broader distribution to lower values in panel (b) that is clearly ascribed to the residual proton contamination. Assuming that most of the estimated PAMELA positron signal is due to misidentified protons means that about two thirds of the associated positron distribution of panel (b) is due to protons. Moreover, test beam data, simulations and prior balloon-borne experiments with a similar calorimeter (see Supplementary Information of [54]) indicate that interacting protons show a rather smooth distribution with no significant structure for this variable, therefore making difficult an interpretation of the distribution at high values of panel (b) as mostly due to protons. Moreover, the imaging calorimeter provide further information about the topology of the energy distribution that can be used for additional rejection. It is reasonable to think that such information can provide an additional factor 100 or so, thus reducing the residual proton contamination to a small amount compared to the signal.

All these uncertainties can be studied and partially resolved only by the use of redundant devices and, especially, multiple measurements performed by systematically different apparata. The agreement between PAMELA and Fermi data gives a good confidence that the increase of the positron flux is indeed to be ascribed to a physical effect and not to systematic effects affecting the measurements. On the other hand, it could be argued that an irreducible contamination in the calorimetry approach for positron identification might affect similarly both the PAMELA and Fermi results. This issue will be resolved by the AMS experiment [53] on board the Interstellar Space Station that will employ a Transition Radiation Detector along with an imaging calorimeter for particle identification.

³Most of the protons do not interact or interact deeply in the calorimeter, hence depositing low amount of energy compared to electrons/positrons of comparable rigidity.

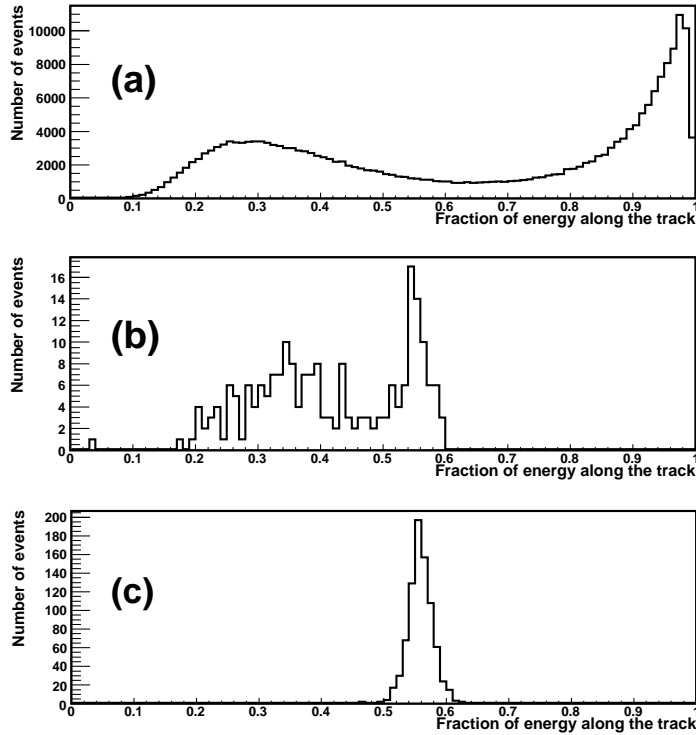


Figure 10: The fraction of calorimeter energy deposited inside a cylinder of radius 0.3 Molière radii in the rigidity region 28–42 GV. Panel (a) shows the distribution for positively-charged particles. Panel (b) and (c) show the same distribution for positively and negatively, respectively, charged particles selected requiring a match between the momentum measured by the tracking system and the total detected energy and the starting point of the shower in the calorimeter. See [101] for more details.

5. Nuclei data

The relative abundances of elements and of isotopes heavier than Helium is another essential piece of information to understand the origin and history of cosmic rays even if heavier nuclei only account for about few percent of the total flux of cosmic rays.

A remarkable resemblance between the the galactic cosmic ray source composition and the abundances found in the solar system can be notice. Both cosmic rays and the solar corona/solar wind show evidence of having undergone chemical alteration, and the resulting fractionation patterns are strikingly similar [104].

However, it has long been recognized that in cosmic rays the observed abundance ratio $(\text{Li}+\text{Be}+\text{B})/(\text{C}+\text{N}+\text{O})$ exceeds the value found in solar system material by a factor of about 10^5 . This difference has been considered to be a measure of how much material cosmic rays have traversed since they were accelerated. Carbon, Nitrogen and Oxigen are considered primary cosmic rays, i.e. nuclei that are produced and accelerated by sources and reach Earth without undergoing fragmentation, while Litium, Berilium and Boron are secondary components resulting from fragmentation reactions in the interstellar medium. Galactic cosmic ray sources and propagation models can be studied measuring the primary and secondary nuclei in the cosmic rays.

In addition to stable isotopes, the cosmic rays contain long-lived radioactive nuclides of either primary or secondary origin. The observed abundances of these “clock” isotopes can be used for establishing various time scales related to the origin of cosmic rays:

- primary isotopes can shed light on the nucleosynthesis process in the cosmic-ray sources. Primary isotopes measured in the cosmic rays have undergone some type of chemical fractionation. It is of major interest studying these isotopes to understand how and where this has occurred [105];
- primary isotopes which decay by electron capture can provide information about the elapsed time between nucleosynthesis and particle acceleration. These types of isotopes are usually called “acceleration delay clocks” [105];
- secondary isotopes which decay by β^\pm emission can measure the average time between the production of these particles and their escape from the Galaxy (“propagation clocks”) [106];

- secondary isotopes which instead decay solely by electron capture can do so only if their velocities have, at some time, been much lower than the velocities at which they are observed. For this reason they are potentially probes of energy changing processes that occur during propagation in the Galaxy (“reacceleration clocks”)[105].

Hence high resolution measurements by cosmic ray nuclei detectors provide very important clues to the astrophysics of our Galaxy and can narrow the range of possible explanations for the origin and propagation history of galactic cosmic rays.

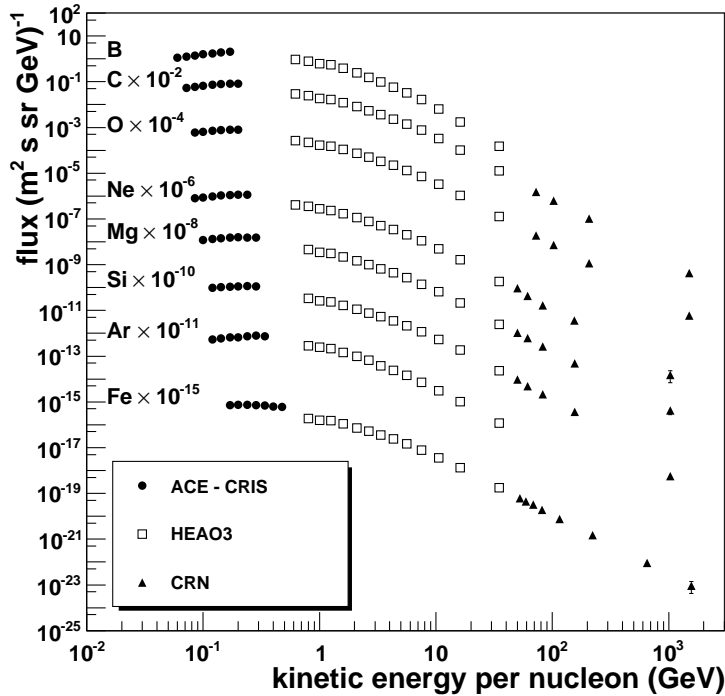


Figure 11: Observed spectra for a selected set of elements as measured by space experiments CRN [107], HEAO-3 [108], ACE (at solar minimum) [109]. To reduce overlap the spectra for individual elements are shifted in vertical direction as indicated.

Figure 11 shows recent nuclei spectra measurements made by the space-based detectors CRN [107], HEAO-3 [108], ACE (at solar minimum) [109]. Notice that the study of a wide energy range nuclei spectra and elemental

composition has been carried out mainly by balloon-borne experiments (for example CREAM [110], ATIC [111] and TRACER [112], not shown in figure). When considering the whole existing data set, a good agreement can be seen between different measurements. At the highest energies the measurement is usually limited by the statistics.

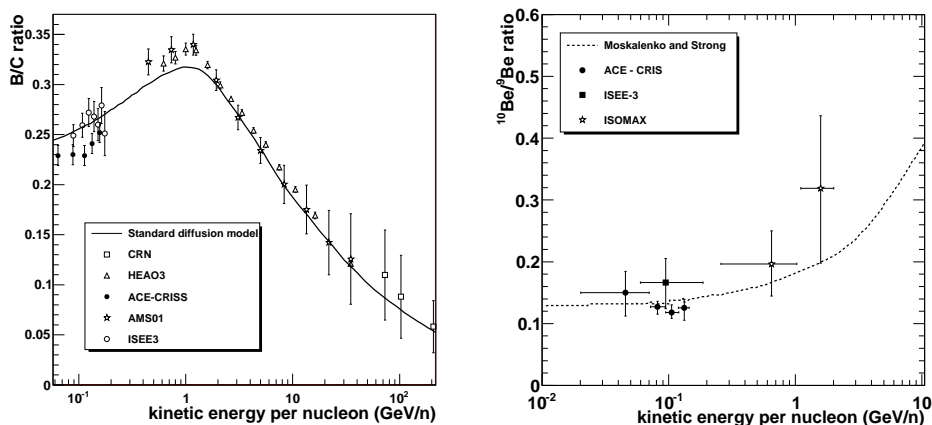


Figure 12: On the left, the B/C fraction as measured by the space experiments ISEE-3 [113], CRN [107], HEAO-3 [108], ACE [114], AMS01 [115]; solid black line is a fit to the data assuming a standard diffusion model [116]. On the right the $^{10}\text{Be}/^9\text{Be}$ ratio as measured by space experiments ACE [114] and ISEE-3 [117] and the balloon-borne experiment ISOMAX [118]; the dotted black line is a diffusive halo model with 4-kpc scale height using GALPROP [119].

In Fig. 12, left panel, the B/C ratio is shown. Since the Boron is expected to be a pure secondary component this ratio is considered a reference for this type of measurements. Moreover, since the major progenitors of B are C, N, and O the production cross sections are better known respect to other secondary nuclei. Solid line in figure represents a fit to the data assuming a Galaxy leaky box model where the chemical composition at sources resembles the solar like abundances. The set of parameters found fitting B/C is in general consistent with all other secondary/primary ratios. Different models (standard or turbulent diffusion models, wind model, minimal re-acceleration model) cannot be distinguished by these data alone. All these models can be used to determine the injection spectral index of primary nuclei which is found to be in the range 2.3 – 2.4 for C and Fe in the energy range 0.5 – 100 TeV [116].

The break at low energies in the B/C ratio is a puzzling feature for which many explanations have been proposed. It has been claimed that HEAO-3 data combined to Voyager 2 show that the break is due to a solar modulation effect [120]. Another possibility is the reacceleration of nuclei which can explain the shape of the B/C ratio with a plausible fit and without the need of ad-hoc break in the diffusion coefficient. The reacceleration models are the favoured ones, since some level of reacceleration is expected when diffusion occurs on moving scatterers. Another simpler explanation of the B/C energy dependence is the local-source model [114, 121], in which a local component of primary cosmic rays is assumed. Since the contribution of local secondaries can be considered negligible, a steep local primary source can eventually make the B/C decrease at low energy.

Figure 12, right panel, shows the $^{10}\text{Be}/^9\text{Be}$ ratio compared to the diffusive halo model obtained using GALPROP. This type of radioactive secondaries (propagation clocks) can only travel a few hundred parsec before decaying; by the mean of these measurements it is possible to determine the diffusion coefficient. Assuming that the diffusion coefficient does not vary from the local region to the full galaxy volume, using the secondary to primary ratio, it is possible to estimate the size of the full propagation region. Given the present measurements, typical results are $D_{xx} \sim 4 \times 10^{28} \text{ cm}^2 \text{ s}^{-1}$ (at 3 GV) for the diffusion coefficient and $z_h = 4 \text{ kpc}$ [116] for the height of the propagation region.

A comprehensive set of “acceleration delay” and “reacceleration” clocks have been measured by the ACE detector. Results on the Co and Ni isotopes seem to be consistent with a delay $\geq 10^5 \text{ y}$ from the synthesis to the acceleration. This observation is not in agreement with models in which the supernova accelerate their own ejecta and seems pointing to the acceleration of existing interstellar matter [116]. Results on reacceleration clock isotopes, like V, Cr and Ti, usually seems to be better in agreement with models including reacceleration, however measurements are not always consistent [116].

Nuclei measurements have been performed over the years using different techniques: energy loss detectors (ISEE-3 [122], ACE-CRIS [104]), Cherenkov detectors (HEAO-3 [123]), Transition Radiation Detector (CNR [124]), magnetic spectrometers (AMS-01 [63], PAMELA [26]).

The nuclei charge identification is usually achieved by measuring the ionization losses in scintillators or silicon detectors, but also other techniques have been adopted, for example Cherenkov counters or TRDs. Experiments

dedicated to the study of nuclei have redundant charge detectors that make the nuclei selection very clean. However, more challenging is the efficiency determination of the particles selection. Nuclei, in fact, can interact within the detector not only producing a hadronic shower but also undergoing a fragmentation into lighter nuclei. The ability and the efficiency of the detector in discarding these type of events can usually only be tested making use of simulations or test beam data. Systematic uncertainties are hence introduced, since simulations suffer the sometimes poor knowledge of cross-sections for “uncommon” nuclei in the desired energy range, while test beam data must be tuned to nominal working conditions of flight detectors and again it is not always possible to have beams of the full range of nuclei and energies.

The nuclei energy measurement technique depends on the energy range that has to be covered. At low energy, up to about 1 GeV/n, non-interacting stopping nuclei are selected and their energy released measured making use of homogeneous calorimetry measurements. The main issues of this approach are the ability of the detector of selecting pure samples of non-interacting particles and the efficiency determination of this selection. Nuclei spallation can potentially be a source of contamination of lower Z nuclei from higher Z ones when the nuclei selection is based only on the energy release. For example it can be difficult to distinguish a Boron nucleus from a Carbon which by spallation has lost a proton which is traveling along the same trajectory – Carbon has charge six, it would release an energy proportional to Z_C^2 but losing a proton it will become a Boron releasing energy proportional to $Z_B^2 = (Z_C - 1)^2$ plus a proton releasing order of one MIP per detector for a total of $(Z_C - 1)^2 + 1$ which has to be compared to the release of $Z_B^2 = (Z_C - 1)^2$ of a single primary Boron.

In the same energy range also the time of flight has been used to determine the nucleus velocity. Slow-down effects in this case must be taken into account and are a source of systematic uncertainties. At higher energies, from the GeV/n to tens of GeV/n, the energy can be measured using Cherenkov detectors and the logarithmic rise of ionization losses detectors, the latter one providing a low energy resolution. A Cherenkov detectors hodoscope has been used in the HEAO-3 experiment [108]. Providing multiple energy measurements an excellent control of systematics errors has been obtained. At the higher energies transition radiation detectors and magnetic spectrometers have been used. In the case of magnetic spectrometers the nuclei energy measurement requires a dedicated calibration of the detector.

Usually the high level emission of delta rays while passing through position measurement detectors can induce a distortion of the recorded cluster which must be identified and taken into account. Moreover, high energy releases, for high Z or very slow nuclei, can saturate the detected signal worsening the position resolution and hence the energy resolution. At the highest energies deep calorimeters must be used. At very high energies nuclei interaction cross section become not-negligible and most of the nuclei interact when entering a calorimeter. Energy released is usually proportional to the incoming particle energy for very deep homogeneous calorimeters. Weight and space constraint of space experiment usually force the use of calorimeters of limited dimension. In this case transversal and longitudinal leakage must be properly taken into account. Indeed multiple energy measurements are needed for dedicated nuclei experiments in order to cover the largest possible energy window and being able of performing an energy cross calibration of detectors with different systematics.

The space-borne experiment PAMELA was also designed to study the abundances and composition of light cosmic rays (up to oxygen) over almost three decades of energy. The PAMELA time of flight (ToF) consist of three scintillator double layers which enable independent charge determinations. Multiple energy deposit measurements combined with the velocity determined by the ToF and with the nuclei rigidity as measured by the tracking system can provide redundant information that improve significantly the charge resolution.

Moreover, even if the PAMELA instruments is optimized for the detection of positrons and antiprotons, three different detectors (ToF, tracker and calorimeter) are able to identify, with different efficiencies, resolutions and Z ranges, light nuclei. Hence it is possible to perform a highly accurate charge measurement by selecting particles independently with the three detectors. The nuclei spectra can be measured up to different momentum depending on the charge since the tracking system resolution depends on the nuclei rigidity.

By comparing the ToF charge measurement with the particle rigidity the different nuclei separated into different bands, as shown in Fig. 13, on the top. By fitting these bands and projecting the signal along the fit lines it is possible to determine the charge resolution. The charge gaussian distribution has a standard deviation that is less than 0.1 for protons and 0.16 for C (in units of proton charge e). A good charge separation can also be obtained comparing the energy released on the first calorimeter plane versus the rigidity as measured by the tracking system, Fig. 13, on the bottom.

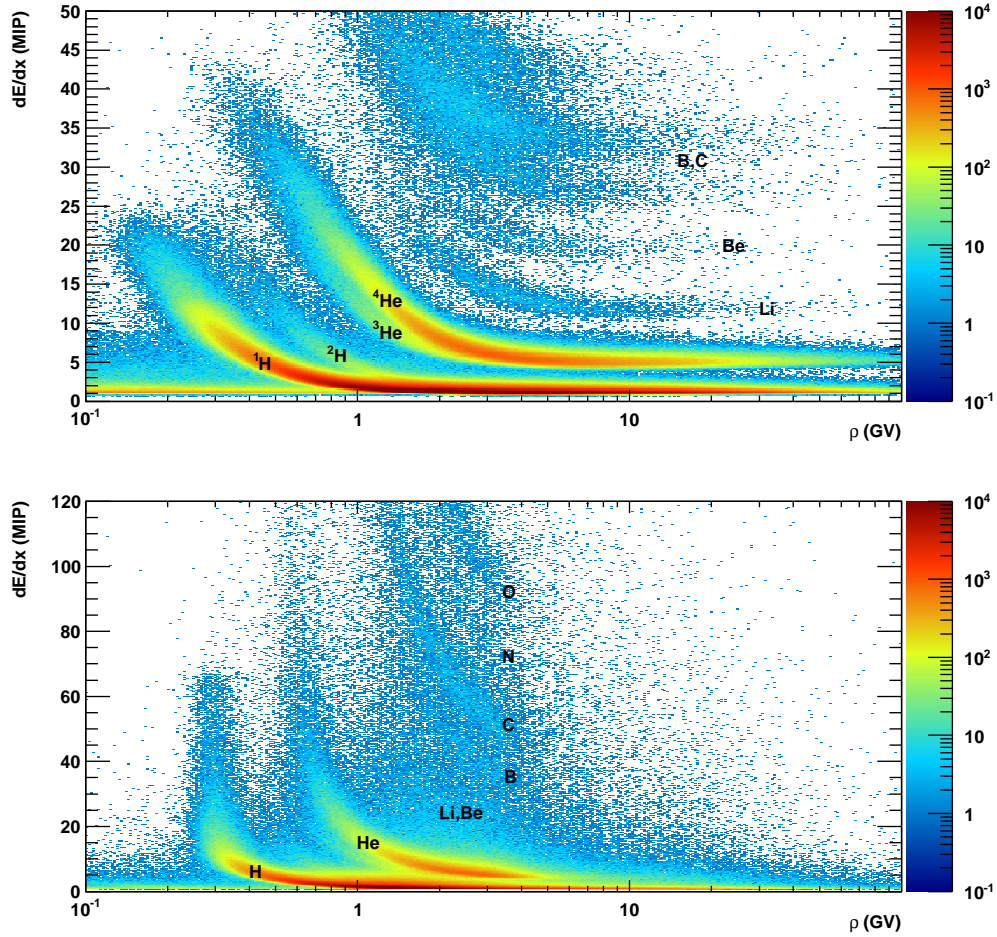


Figure 13: The nuclei separation capabilities of PAMELA ToF (top) and calorimeter (bottom) [51].

In this latter case charges higher than Oxygen can be separated since the dynamic range in MIP of the calorimeter strips is much bigger than the ToF and tracker ones.

Below ~ 2 GeV/n, three independent energy measurements are available: the time of flight, the deflection of the particle in the spectrometer magnetic field, the Bragg's peak of the nucleus stopping in the calorimeter. In this energy region is therefore possible to put constraints on the tracking system systematics errors in the energy measurements. Moreover a cross-check of

nuclei selection efficiencies as function of the nuclei energy can be used to estimate systematics in the nuclei separation. To extend the nuclei measurement at higher energies (hundred of GeV/n) the tracking system must be used to measure the particle rigidity.

The PAMELA B/C ratio will be a very important measurement to put strong constraints on cosmic-ray propagation and acceleration models. In fact, the use of a full data set (matter, anti-matter and nuclei over a wide energy range) provided by a single instrument permit to avoid inconsistencies between data sets from different experiments and minimize uncertainties on the solar modulation parameters which is difficult to parametrize properly.

6. Future

On the 19th of May 2011 the AMS-02 apparatus [53] was installed on-board the International Space Station (ISS) and it started collecting data. The apparatus resembles the PAMELA one being equipped with a permanent magnet, a silicon tracking device and an electromagnetic calorimeter. However, AMS has a significantly larger acceptance (about a factor 20) and additional detectors such as a Transition Radiation Detector and a Ring Imaging Cherenkov detector that will provide a significant improvement in statistics and systematics respect to PAMELA concerning antiparticle and chemical composition of the cosmic radiation.

Another experiment designed to study the electron component and the chemical composition of the cosmic radiation with a calorimetry approach is CALET [76]. The apparatus is built around a 30 radiation length calorimeter and it will be placed on board the ISS sometime around 2014. Major scientific objectives are to search for nearby cosmic ray sources and dark matter. With an acceptance of about $0.12 \text{ m}^2\text{sr}$, CALET will be able to precisely measure the all-electron energy spectrum from 20 GeV to 10 TeV. Though not optimized for hadrons, CALET has also a capability to measure protons and nuclei up to 1000 TeV, and will have a function to monitor solar activity and γ ray bursts with additional instrument. CALET expects to measure ~ 20 protons and ~ 15 nuclei of the iron family above 5×10^{14} eV in a five years mission.

A similar calorimetry approach will be employed by Gamma-400 [77] to study the high-energy gamma-ray flux and cosmic-ray electrons and nuclei. The apparatus will be placed on board a Russian satellite, which launch is foreseen for 2017-2018. With a similarly deep but significantly larger calorimeter (acceptance of about $1 \text{ m}^2\text{sr}$), Gamma-400 will be able to increase by about an order of magnitude the statistics acquired by CALET.

The energy region close to the knee (located at $\sim 3\text{-}4$ PeV) turns out to be very difficult to explore with balloons or space borne instruments, due to the very low cosmic ray fluxes (2-3 particles per $\text{m}^2\text{sr yr}$ for $E > 10^{16}$ eV) and the need to provide an energy measurement with a mass limited instrument. To obtain a statistically significant data sample to study the spectral index change, across the knee region, requires a large collection power and it is only possible with a long duration space experiment.

Taking advantage of a long observation time and a quite large geometric factor, Gamma-400 can extend spectral measurements and studies of cosmic

ray elemental composition in energy and provide high precision data at lower energies.

All together the new set of future measurements with higher statistics and in a wider energy range will provide an important tool for testing the theoretical scenarios developed to explain the data published recently by PAMELA, Fermi and contemporary balloon-borne experiments.

A even more important contribution to the understanding of present day cosmic ray measurements will come from observations and discoveries made with man made accelerators, like LHC. If new physics scenarios will be reachable and studied at accelerators it will be possible cross-check theoretical models and predict effects measurable in cosmic ray astroparticle physics.

7. Acknowledgements

We would like to thank the PAMELA Collaboration for providing some of the information included in this paper and V. Formato for helping in the compilation of this paper.

References

- [1] V. L. Ginzburg, S. I. Syrovatskii, *The Origin of Cosmic Rays*, New York: Macmillan, 1964.
- [2] W. Baade, F. Zwicky, in: *Proc. Nat. Acad. of Sciences of United States of America* (1934), volume 20, p. 259.
- [3] M. A. Malkov, L. O'C. Drury, *Reports on Progress in Physics* 64 (2001) 429–481.
- [4] G. E. Allen, et al., *Astrophys. J. Lett.* 487 (1997) L97.
- [5] F. Aharonian, et al., *Nature* 432 (2004) 675.
- [6] F. Aharonian, et al., *Astron. Astrophys.* 464 (2007) 235.
- [7] T. A. Porter, I. V. Moskalenko, A. W. Strong, *Astrophys. J. Lett.* 648 (2006) L29.
- [8] D. C. Ellison, D. J. Patnaude, P. Slane, J. Raymond, *Astrophys. J.* 712 (2010) 287.
- [9] Y. Uchiyama, F. A. Aharonian, T. Tanaka, T. Takahashi, Y. Maeda, *Nature* 449 (2007) 576.
- [10] M. Tavani, et al., *Astrophys. J. Lett.* 710 (2010) L151.
- [11] A. A. Abdo, et al., *Science* 327 (2010) 1103.
- [12] A. W. Strong, I. V. Moskalenko, *Astrophys. J.* 509 (1998) 212.
- [13] F. C. Jones, A. Lukasiak, V. Ptuskin, W. Webber, *Astrophys. J.* 547 (2001) 264.
- [14] F. Donato, et al., *Astrophys. J.* 563 (2001) 172.

- [15] M. Amenomori, et al., *Science* 314 (2006) 439.
- [16] A. A. Abdo, et al., *Astrophys. J.* 698 (2009) 2121.
- [17] R. Abbasi, et al., *Astrophys. J.* 718 (2009) L194.
- [18] B. Bartoli, et al., *Phys. Rev. D* 85 (2012) 092005.
- [19] D. Caprioli, E. Amato, P. Blasi, *Astropart. Phys.* 33 (2010) 160.
- [20] P. Blasi, E. Amato, *J. of Cosmology and Astrop. Phys. (JCAP)* 1201 (2012) 010.
- [21] G. B. Khristiansen, G. V. Kulikov, *Zhurn. Experm. Teor. Fiz.* 35 (1958) 635.
- [22] P. O. Lagage, C. J. Cesarsky, *Astron. Astrophys.* 118 (1983) 223.
- [23] J. R. Hörandel, *Astropart. Phys.* 21 (2004) 241.
- [24] O. Adriani, et al., *Science* 106 (2011) 201101.
- [25] H. S. Ahn, et al., *Astrophys. J. Lett.* 714 (2010) L89.
- [26] P. Picozza, et al., *Astropart. Phys.* 27 (2007) 296.
- [27] M. Boezio, et al., *Astrophys. J.* 518 (1999) 457.
- [28] J. Buckley, et al., *Astrophys. J.* 429 (1994) 736.
- [29] K. Asakimori, et al., *Astrophys. J.* 502 (1998) 278.
- [30] M. Garcia-Munoz, G. M. Mason, J. A. Simpson, *Astrophys. J. Lett.* 201 (1975) L145.
- [31] N. De Simone, Galactic and solar proton flux measurements in the energy range 80 MeV - 1.2 TeV with the PAMELA space experiment, Ph.D. thesis, University of Rome “Tor Vergata”, Rome, Italy, 2011. <http://pamela.roma2.infn.it/>.
- [32] M. S. Potgieter, *J. Plasma Fusion Res.* 8 (2009) 132.
- [33] T. Delahaye, J. Lavalle, R. Lineros, F. Donato, N. Fornengo, *Astron. Astrophys.* 524 (2010) A51.

- [34] W. Menn, et al., *Astrophys. J.* 533 (2000) 281.
- [35] M. Boezio, et al., *Astropart. Phys.* 19 (2003) 583.
- [36] S. Haino, et al., *Phys. Lett. B* 594 (2004) 35.
- [37] J. P. Wefel, et al., in: *Proc. 30th Int. Cosmic Ray Conf. (Merida 2007)*, volume 2, p. 31.
- [38] J. Alcaraz, et al., *Phys. Lett. B* 490 (2000) 27.
- [39] V. I. Zatsepin, N. V. Sokolskaya, *Astron. Astrophys.* 458 (2006) 1.
- [40] P. L. Biermann, *Astron. Astrophys.* 271 (1993) 649.
- [41] G. D'Agostini, *Nucl. Instrum. Meth. A* 362 (1995) 487.
- [42] J. Alcaraz, *Phys. Lett. B* 461 (1999) 387.
- [43] M. Boezio, V. Bonvicini, E. Mocchiutti, P. Schiavon, G. Scian, A. Vacchi, G. Zampa, N. Zampa, *Nucl. Instrum. Meth. A* 487 (2002) 407.
- [44] W. R. Webber, *Adv. Space Res.* 19 (1997) 755.
- [45] W. R. Webber, et al., *Astrophys. J.* 380 (1991) 230.
- [46] J. J. Beatty, et al., *Astrophys. J.* 413 (1993) 268.
- [47] J. P. Wefel, et al., in: *Proc. 24th Int. Cosmic Ray Conf. (Rome 1995)*, volume 2, p. 630.
- [48] G. A. de Nolfo, et al., in: *AIP Conference Proceedings (2005)*, volume 528, p. 425.
- [49] J. Z. Wang, et al., *Astrophys. J.* 564 (2002) 244.
- [50] M. Aguilar, et al., *Astrophys. J.* 736 (2011) 105.
- [51] V. Formato, et al., in: *Proc. 32nd Int. Cosmic Ray Conf. (Beijing 2011)*.
- [52] P. Papini, et al., *Astrophys. J.* 615 (2004) 259.

- [53] R. Battiston, et al., in: Proc. 29th Int. Cosmic Ray Conf. (Pune 2005), volume 10, p. 151.
- [54] O. Adriani, et al., Nature 458 (2009) 607.
- [55] A. M. Atoyan, F. A. Aharonian, H. J. Volk, Phys. Rev. D 52 (1995) 3265.
- [56] M. Cirelli, M. Kadastik, M. Raidal, A. Strumia, Nucl. Phys. B 813 (2008) 1.
- [57] J. Nishimura, et al., Astrophys. J. 238 (1980) 394.
- [58] F. Aharonian, et al., Phys. Rev. Lett. 101 (2008) 261104.
- [59] J. Chang, et al., Nature 456 (2008) 362.
- [60] M. Ackermann, et al., Phys. Rev. D 82 (2010) 092004.
- [61] O. Adriani, et al., Phys. Rev. Lett. 332 (2011) 69.
- [62] M. Boezio, et al., Astrophys. J. 532 (2000) 653.
- [63] J. Alcaraz, et al., Phys. Lett. B 484 (2000) 10.
- [64] M. A. DuVernois, et al., Astrophys. J. 559 (2001) 296.
- [65] C. Grimani, et al., Astron. Astrophys. 392 (2002) 287.
- [66] T. Kobayashi, J. Nishimura, Y. Komori, T. Shirai, N. Tateyama, T. Taira, K. Yoshida, T. Yuda, in: Proc. 26th Int. Cosmic Ray Conf. (Salt Lake City 1999), volume 3, p. 61.
- [67] S. Torii, et al., Astrophys. J. 559 (2001) 973.
- [68] V. S. Ptuskin, et al., Astrophys. J. 642 (2006) 902.
- [69] L. J. Gleeson, W. I. Axford, Astrophys. J. 154 (1968) 1011.
- [70] A. A. Abdo, et al., Phys. Rev. Lett. 102 (2009) 181101.
- [71] M. Ahlers, P. Mertsch, S. Sarkar, Phys. Rev. D 80 (2009) 123017.
- [72] P. Blasi, Phys. Rev. Lett. 103 (2009) 051104.

- [73] P. Serpico, 2011. Review Paper in this Special Issue.
- [74] O. Adriani, et al., *Astropart. Phys.* 34 (2010) 1.
- [75] M. Ackermann, et al., *Phys. Rev. Lett.* 108 (2012) 011103.
- [76] S. Torii, et al., *J. Phys. Conf. Ser.* 120 (2008) 062020.
- [77] A. M. Galper, et al., *Astrophys. Space Sci. Trans.* 7 (2011) 75.
- [78] T. K. Gaisser, E. H. Levy, *Phys. Rev. D* 10 (1974) 1731.
- [79] R. J. Protheroe, *Astrophys. J.* 254 (1982) 391.
- [80] J. A. D. Shong, R. H. Hildebrand, P. Meyer, *Phys. Rev. Lett.* 12 (1964) 3.
- [81] R. L. Golden, et al., *Phys. Rev. Lett.* 43 (1979) 1196.
- [82] E. A. Bogomolov, et al., in: *Proc. 16th Int. Cosmic Ray Conf. (Kyoto 1979)*, volume 1, p. 330.
- [83] A. Buffington, S. M. Schindler, C. R. Pennypacker, *Astrophys. J.* 248 (1981) 1179.
- [84] O. Adriani, et al., *Phys. Rev. Lett.* 105 (2010) 121101.
- [85] M. Boezio, et al., *Astrophys. J.* 487 (1997) 415.
- [86] M. Boezio, et al., *Astrophys. J.* 561 (2001) 787.
- [87] A. S. Beach, et al., *Phys. Rev. Lett.* 87 (2001) 271101.
- [88] Y. Asaoka, et al., *Phys. Rev. Lett.* 88 (2002) 051101.
- [89] K. Abe, et al., *Phys. Lett. B* 670 (2008) 103.
- [90] M. Aguilar, et al., *Phys. Rep.* 366 (2002) 331.
- [91] K. Abe, H. Fuke, S. Haino, T. Hams, M. Hasegawa, et al., *Phys. Rev. Lett.* 108 (2012) 051102.
- [92] F. Donato, D. Maurin, P. Brun, T. Delahaye, P. Salati, *Phys. Rev. Lett.* 102 (2009) 071301.

- [93] M. Ambrosio, et al., *Astropart.Phys.* 20 (2003) 145.
- [94] M. Amenomori, et al., *Astropart. Phys.* 28 (2007) 137.
- [95] G. Di Sciascio, et al., *Nucl. Instrum. Meth. A* 630 (2011) 63.
- [96] R. L. Golden, et al., *Astrophys. J.* 457 (1996) L103.
- [97] S. W. Barwick, et al., *Astrophys. J.* 482 (1989) L191.
- [98] J. Clem, P. Evenson, in: *Proc. 30th Int. Cosmic Ray Conf. (Pune 2007)*.
- [99] M. Aguilar, et al., *Phys. Lett. B* 646 (2007) 145.
- [100] U. W. Langner, M. S. Potgieter, *Adv. Space Res.* 34 (2004) 144.
- [101] M. Boezio, et al., *New J. Phys.* 11 (2009) 105023.
- [102] S. A. Stephens, *Astropart. Phys.* 6 (1997) 229.
- [103] K. Nakamura, et al., *J. Phys. G* 37 (2010) 075021.
- [104] E. C. Stone, et al., *Space Sci. Rev.* 86 (1998) 283.
- [105] R. A. Mewaldt, et al., *Space Sci. Rev.* 99 (2001) 27.
- [106] V. S. Ptuskin, A. Soutoul, *Space Sci. Rev.* 86 (1998) 225.
- [107] D. Müller, et al., *Astrophys. J.* 374 (1991) 356.
- [108] J. J. Engelmann, et al., *Astr. Astr.* 233 (1990) 96.
- [109] J. S. George, et al., *Astrophys. J.* 698 (2009) 1666.
- [110] H. S. Ahn, et al., *Astropart. Phys.* 30-3 (2008) 133.
- [111] A. D. Panov, et al., in: *Proc. 30th Int. Cosmic Ray Conf. (Merida 2007)*, volume 2, p. 3.
- [112] M. Ave, et al., *Astrophys. J.* 697 (2009) 106.
- [113] R. A. Leske, et al., *Astrophys. J.* 405 (1993) 567.

- [114] A. J. Davis, et al., in: *Acceleration and Transport of Energetic Particles Observed in the Heliosphere: ACE 2000 Symposium*. AIP Conference Proceedings, volume 528, p. 421.
- [115] N. Tomassetti, et al., arXiv:1106.2268, 2011.
- [116] A. W. Strong, I. V. Moskalenko, V. S. Ptuskin, *Ann. Rev. Nucl. Part. Sci.* 57 (2007) 285.
- [117] M. E. Wiedenbeck, D. E. Greiner, *Astrophys. J.* 239 (1980) L139.
- [118] T. Hams, et al., *Astrophys. J.* 611 (2004) 892.
- [119] A. W. Strong, I. V. Moskalenko, *Adv. Space Res.* 27 (2001) 717.
- [120] W. R. Webber, F. B. McDonald, A. Lukasiak, *Astrophys. J.* 599 (2003) 582.
- [121] I. V. Moskalenko, A. W. Strong, S. J. Mashnik, J. F. Ormes, *Astrophys. J.* 586 (2003) 1050.
- [122] D. E. Greiner, F. S. Bieser, H. H. Heckman, *IEEE Trans. Geosci. Electronics GE-16* (1978) 163.
- [123] M. Bouffard, et al., *Astrophys. and Space Sci.* 84 (1982) 3.
- [124] S. P. Swordy, et al., *Astrophys. J.* 349 (1990) 625.